Variable temperature ^{93}Nb NMR investigation of local structure and polar nanoclusters in lead magnesium niobate/lead scandium niobate solid solutions

Robert L. Vold,[1,*] Gina L. Hoatson,[2] and M. Vijayakumar[2]
[1]*Department of Applied Science, College of William and Mary, Williamsburg, Virginia 23187, USA*
[2]*Department of Physics, College of William and Mary, Williamsburg, Virginia 23187, USA*
(Received 29 December 2006; published 23 April 2007)

^{93}Nb magic angle spinning (MAS) and three quantum magic angle spinning (3QMAS) NMR experiments have been performed on $(1-x)PbMg_{1/3}Nb_{2/3}O_3$-$xPb_{1/2}Sc_{1/2}NbO_3$ [$(1-x)$PMN-xPSN] ordered samples, for compositions $x=0.6$ (a normal ferroelectric) and 0.2 (a relaxor). Deconvolution of the MAS spectra at several temperatures ranging from 245 to 375 K reveals seven narrow peaks, P0,P1,…,P6, and two broad components, D1 and D2, that are assigned to specific local Nb^{5+} environments defined by the identities of the six nearest *B*-site cations. For both sample compositions, the temperature dependence of peak positions, MAS intensities, and linewidths is weak for peaks P0,P1,…,P6 and D2. However, the peak position, linewidth, and integrated intensity of D1 show anomalies in the range of the paraelectric to ferroelectric phase transition, that are much sharper for $x=0.6$ than for $x=0.2$. These effects are associated with the local structure and dynamics of polar nanoclusters. Site-specific values of the quadrupole product and isotropic chemical shift are extracted from combined analysis variable temperature MAS and 3QMAS spectra of the 0.4PMN-0.6PSN sample.

DOI: 10.1103/PhysRevB.75.134105 PACS number(s): 76.60.−k, 82.56.−b, 77.84.Dy, 77.80.−e

I. INTRODUCTION

Ferroelectric perovskites, such as lead magnesium niobate $PbMg_{1/3}Nb_{2/3}O_3$ (PMN) and its solid solutions with lead titanate $PbTiO_3$, lead zirconium titanate $Pb(Zr_{1/2}Ti_{1/2})O_3$, and lead scandium niobate $PbSc_{1/2}Nb_{1/2}O_3$ (PSN), have led to many useful devices that take advantage of their large piezoelectric coefficients and high remnant electric polarization.[1,2] Relaxor ferroelectrics are characterized by a broad, frequency dependent temperature of maximum dielectric permittivity ($T_M \sim 285$ K in PMN), and a diffuse transition into the relaxor ferroelectric state below T_M.[2] This behavior is fundamentally different from that of normal ferroelectrics, which exhibit a sharp paraelectric to ferroelectric transition with a frequency independent transition temperature. It is generally agreed that local polarization, resulting from structural and chemical disorder, plays a crucial role in relaxor behavior.[2,3] Several models have been proposed to relate local, microscopic polarization to the gradual onset of macroscopic polarization, including superparaelectric glasses,[4] dipole glasses,[5] and random-bond–random- field interactions.[6] However, the microscopic origins of relaxor ferroelectricity are still not fully understood. In this regard, experimental characterization of local, nanoscale structural changes occurring throughout the relaxor ferroelectric transition region should be very informative.

The system $(1-x)PbMg_{1/3}Nb_{2/3}O_3$-$xPb_{1/2}Sc_{1/2}NbO_3$ provides a particularly well studied example of relaxor behavior associated with *B*-site disorder.[7,8] Temperature dependent extended x-ray-absorption fine structure studies of pure PMN and PSN (Ref. 9) reveal distributions of Nb-O internuclear distances, indicating that the Nb^{5+} ions are off center from their ideal perovskite lattice positions by as much as 0.1 Å. This is comparable in magnitude to the more well-known Pb^{2+} ion displacements.[10] In crystalline materials, there are well established empirical correlations between NMR parameters of both ^{207}Pb (Ref. 11) and ^{95}Nb (Ref. 12) with bond lengths, coordination number, and degree of bond hybridization. Thus, it is not surprising that NMR of these nuclei can provide a wealth of information about local structure in relaxors. For example, recent ^{207}Pb NMR measurements on single-crystal samples of pure PMN ($x=0$) and pure PSN ($x=1$), cooled in strong static electric fields, were correlated with dielectric relaxation measurements over a wide temperature range. The results were discussed in terms of atomic level structure and dynamics of polar nanoclusters in these materials.[13,14]

Unlike pure PMN, $(1-x)$PMN-xPSN solid solutions exhibit 1:1 *B*-site "chemical order" along the ⟨111⟩ direction. The stoichiometric formula that corresponds to this random site model is $Pb(\beta'_{1/2}\beta''_{1/2})O_3$, where β' denotes a random mixture $[Mg^{2+}_{2(1-x)/3}Sc^{3+}_{x}Nb^{5+}_{(1-x)/3}]$ and β'' denotes Nb^{5+} alone. β'' planes, containing exclusively Nb^{5+} cations, alternate along the ⟨111⟩ direction with β' planes that contain a random mixture of Mg^{2+}, Sc^{3+}, and Nb^{5+} cations. Half of the *B* cations are on β' sites, and half are on β'' sites. Each Nb^{5+} cation is surrounded by a (distorted) octahedron of oxygen O^{2-} anions, 6 or 12 Pb^{2+} ions, and a shell of 6 nearest *B*-site neighbor cations. Following Ref. 15, the nearest *B*-site neighbor (nBn) configurations are designated by the numbers of Mg^{2+}, Sc^{3+}, and Nb^{5+} cations (N_{Mg}, N_{Sc}, N_{Nb}); each number can range from 0 to 6 with the constraint that their sum is 6. The probability of any particular configuration, and hence its expected integrated intensity in the MAS spectrum, is readily calculated by procedures given in Ref. 15.

Careful thermal annealing of the samples leads to the formation of relatively large ordered domains (~300 nm for $x=0.6$).[7] For $x \leqslant 0.5$, the ordered samples exhibit typical relaxor behavior, but for higher PSN concentrations a normal (nonrelaxor) paraelectric-ferroelectric transition is observed.[7] For disordered (unannealed) samples, relaxor behavior is observed over the range of compositions $0 \leqslant x \leqslant 0.9$.[8] It is generally accepted that *B*-site compositional disorder is a requirement for relaxor behavior,[3] but the complex behavior of

PMN-PSN solid solutions illustrates the need for a more detailed understanding of how specific local *B*-site ion configurations facilitate the cooperative evolution of short-range polar distortions into larger, aligned ferroelectrically active domains with macroscopic remnant polarization.

Solid-state NMR is an excellent tool to probe this question due to its high sensitivity to the local environment.[16,17] Since the ^{93}Nb nucleus has spin $I=9/2$, the dominant NMR interactions are the quadrupole coupling and isotropic chemical shifts, δ_{iso}^{CS}. When expressed in ppm, the chemical shift is independent of magnetic field, while both the second-order isotropic quadrupole-induced shift (δ_{iso}^{2Q}) and the linewidth of the central transition are inversely proportional to the square of the magnetic field. This means that higher magnetic fields result in better spectral resolution, especially when combined with fast magic angle spinning (MAS) and multiple quantum MAS experiments. Glinchuk *et al.* have studied the PMN-PSN system using stationary samples at low magnetic fields,[18] but the inherent disorder found even in single crystals[19] leads to low spectral resolution that precluded definitive identification of specific configurations.

In previous ^{93}Nb NMR investigations of solid solutions of $(1-x)$PMN-xPSN at ambient temperature and 19.6 T for both annealed and unannealed samples, we identified the 28 configurations of next-nearest B-site neighbors predicted according to the random site model, and assigned several partially resolved spectral lines to specific configurations on the basis of self-consistent analyses of MAS and multiple quantum MAS (MQ MAS) spectra measured as a function of overall composition.[15,20] In this paper, we analyze temperature dependent MAS and MQMAS spectra of annealed samples for $x=0.6$ and 0.2, and compare the results with similar measurements on pure PMN.[21] The aim is to confirm the conclusion[21] that certain nBn configurations are involved in polar nanoclusters while others are not, and to see which specific nBn configurations are most important for the composition dependent change from relaxor to normal ferroelectric behavior as scandium content increases.

II. EXPERIMENTAL METHODS

The $(1-x)$PMN-xPSN samples were provided by Dr. Peter Davies (University of Pennsylvania) and are the same materials used previously for ambient temperature ^{93}Nb MAS investigations.[15] They have been well characterized by x-ray diffraction, transmission electron microscopy, and dielectric measurements.[7,8,22] Both samples used in the present study were thermally annealed (ordered) to better than 95% as determined by x-ray diffraction.[7,8,22]

^{93}Nb MAS spectra were obtained at 17.6 T (^{93}Nb resonance frequency $\upsilon_L=183.61$ MHz) using a Bruker Avance NMR spectrometer. Samples were contained in 2.5 mm rotors and spun at 30 kHz to avoid overlap between the central $(1/2\rightarrow-1/2)$ transition and satellite transition sideband manifolds. Typically, the number of scans used in the MAS experiments was 4096, the full spectral width was 500 kHz, and 4096 complex data points were collected. 1 μs pulses with amplitude of 50 kHz were used at all temperatures, and a recycle delay of 400 ms was sufficient to ensure full recovery between scans. MAS spectra were obtained at several temperatures in the range 245–375 K, regulated by a Bruker temperature controller with precision better than ±0.2 K. Due to frictional heating by the spinner drive gas, the true sample temperature is higher than each controller set point by 30±1 K. This correction was determined by calibrating our 2.5 mm probe using separate rotors containing lead nitrate and a fixed-point reference (deuterated stearic acid, which melts at 341 K). Reference spectra of $NbCl_5$ in acetonitrile solution were recorded periodically to check referencing and compensate for field drift (which was found to be negligible, typically less than 2 proton Hz/h). Reported ^{93}Nb peak positions are accurate within ±1.0 ppm, and are referenced to the chemical shift of $NbCl_5$ in acetonitrile solution, $\delta_{iso}^{CS}=0$ ppm.

The three-pulse Z-filter three quantum MAS (3Q MAS) sequence[23] was necessary for ^{93}Nb experiments because of short $T_1(<50$ ms) and $T_2(<0.5$ ms) relaxation times. The rf field strength was 75 kHz for the first two pulses, and 10 kHz for the third (selective) pulse. The interval between the second and third pulses was synchronized to one rotor period, 33.33 μs. 1024 complex data points were collected with dwell time of 14 μs in the direct acquisition dimension; 62 time increments of $\Delta t_1=28$ μs were used in the indirect acquisition dimension; and 2000 scans were accumulated with a 250 ms relaxation delay. Pure absorption mode spectra in both dimensions were obtained by the States procedure. The indirect and direct frequencies in a 3QMAS experiment, υ_1 and υ_2, respectively, are given in units of ppm by Eq. (1):

$$\upsilon_1 = \frac{1}{1+k}\left[3\delta_{iso}^{cs} + \frac{3P_Q^2}{40\upsilon_L^2 I^2(2I-1)^2}C_0(3/2,I) + 20\frac{\upsilon_Q^2}{\upsilon_L^2}F_4(\alpha,\beta,\eta)C_4(3/2,I) - k\upsilon_2\right], \tag{1a}$$

$$\upsilon_2 = \delta_{iso}^{cs} + \frac{3P_Q^2}{40\upsilon_L^2 I^2(2I-1)^2}C_0(1/2,I) + 20\frac{\upsilon_Q^2}{\upsilon_L^2}F_4(\alpha,\beta,\eta_Q)C_4(1/2,I), \tag{1b}$$

$$P_Q = C_Q(1+\eta_Q^2/3)^{1/2}, \tag{1c}$$

$$\upsilon_Q = \frac{C_Q}{2I(2I-1)}, \tag{1d}$$

where the spin quantum number $I=9/2$ for ^{93}Nb, P_Q is the quadrupole product, η_Q is the asymmetry parameter of the electric-field gradient tensor, and C_Q is the quadrupole coupling constant.[20] The angular factors $F_4(\alpha,\beta,\eta_Q)$ depend on crystallite orientation angles α and β as well as η_Q. Expressions for $F_4(\alpha,\beta,\eta_Q)$ and the coefficients C_0 and C_4 may be found in the literature.[20,24] Equation (1a) includes an arbitrary shearing factor k. Including the scale factor $1/(1+k)$ in this formula implies that the frequency points in υ_1 run from $-1/(2\Delta t_1)$ to $+1/(2\Delta t_1)(1-2/N_1)$ in steps of $1/[2(1+k)N_1\Delta t_1]$, where N_1 is the number of t_1 increments used to

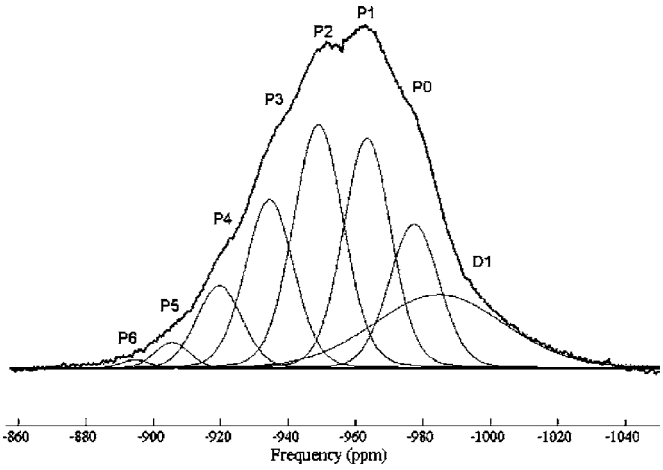

FIG. 1. MAS spectrum of ordered 0.4PMN-0.6PSN at 265 K. The bold solid line is the experimental spectrum, and thin solid lines represent components P0–P6 and D1, determined by deconvolution as described in the text.

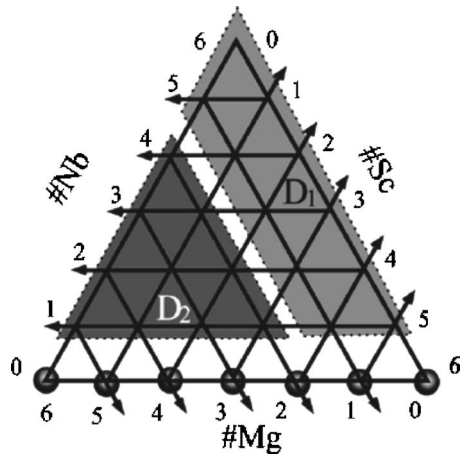

FIG. 2. The 28 nBn configurations of Nb^{+5} cations. For a given grid point, vectors pointing toward each axis indicate the number of each type of cation. Lightly shaded configurations are assigned to "distribution" peak D1 and the darker shaded configurations to peak D2 (for details, see text and Ref. 20). Peaks labeled P0–Pn in Fig. 1 are assigned (Ref. 20) to nBn configurations with $N_{\mathrm{Nb}}=0$, $N_{\mathrm{Mg}}=n$, and $N_{\mathrm{Sc}}=6-n$.

collect the data. Shearing was used in the original 3QMAS experiments[25] to suppress second-order quadrupole broadening caused by the F_4 term, by choosing $k=C_4(3/2,I)/C_4(1/2,I)$. For PMN and other disordered systems, where significant broadening results from a distribution of isotropic chemical shifts, it is more effective to choose $k=3$. This does not fully eliminate the anisotropic quadrupole broadening, but does eliminate all broadening and other effects of the isotropic chemical shift from one-dimensional slices parallel to the F_1 axis. Thus, line-shape slices along F_1 can be used to assess distributions of quadrupole coupling parameters alone.

III. RESULTS

A. 0.4PMN-0.6PSN variable temperature MAS experiments

The central transition $(+1/2\rightarrow 1/2)$ region of a 260 K ^{93}Nb MAS spectrum of 0.4PMN-0.6PSN is shown in Fig. 1.

The sample is in the ferroelectric state, well below the temperature of maximum dielectric permeability, $T_M \simeq 285$ K.[8] Our analysis is confined to the central transition, although manifolds of satellite transition spinning sidebands can be observed out to at least 1 MHz by using wider spectral windows. A MATLAB program was used to deconvolute the central transition into a weighted sum of Gaussian-Lorenztian functions, using procedures similar to those of program DMFIT as described by Massiot *et al.*[26] Our previous study[15] showed that seven narrow components and one broad component are required to fit the line shape for this particular composition.

Following Refs. 15 and 20, each of the 28 nBn configurations $(N_{\mathrm{Mg}},N_{\mathrm{Sc}},N_{\mathrm{Nb}})$ is represented by a point on a triangular grid, as shown in Fig. 2. For a given grid point, the three vectors pointing to the axes indicate the numbers of each type of cation.

The seven narrow components of the spectrum, labeled P0, P1, P2,…,P6 in Fig. 1, correspond to nBn configurations without niobium cations $(N_{\mathrm{Mg}},\ 6-N_{\mathrm{Mg}},\ 0)$, with $N_{\mathrm{Mg}}=0,1,\ldots,6$. These are represented by the seven grid points on the bottom of the triangle in Fig. 2. These assignments[15] are based on the observation that the variation of integrated peak intensities with overall scandium concentration is in accord with the generally accepted random site model[27] of B-site cation ordering. The lines are relatively narrow because similar ionic radii and electronegativities of all six nBn cations (either Sc^{3+} or Mg^{2+}) lead to a more symmetric environment and smaller electric-field gradients at the Nb^{5+} sites.

Size and electronegativity mismatch resulting from substituting Nb^{5+} for Mg^{2+} or Sc^{3+} severely distorts the local environment, leading to larger quadrupole coupling constants and hence greater linewidths. Thus, transitions arising from Nb^{5+} with nBn configurations that contain one or more Nb^{5+} cations are at best only partially resolved, giving rise to two broad "distribution peaks" D1 and D2. D1 has been assigned to the 11 configurations $(N_{\mathrm{Mg}},N_{\mathrm{Sc}},N_{\mathrm{Nb}})$ with $N_{\mathrm{Mg}}=0$ or 1 and at least one Nb neighbor (i.e., $N_{\mathrm{Nb}}\neq 0$), while D2 includes the remaining 10 $N_{\mathrm{Nb}}\neq 0$ configurations with $N_{\mathrm{Mg}}=2,3,4,5$.[20] In MAS spectra of the $x=0.6$ sample at 265 K (Fig. 1), D2 has negligible intensity and was omitted from the fit.

The MAS spectrum of 0.4PMN-0.6PSN in the paraelectric phase, at 360 K, is shown in Fig. 3.

The peaks are all sharper and shifted slightly to high field relative to the 260 K spectrum shown in Fig. 1. This spectrum can be fitted equally well with seven peaks [Fig. 3(a)] or eight peaks [Fig. 3(b)]. Seven partially resolved features are readily assigned to nBn configurations P0,P1,…,P6 by comparison with the 260 K spectrum. If real, the eighth peak can be identified with D1.

The fraction of Nb^{5+} cations residing in each nBn configuration does not change until temperatures much higher than those attainable in this study, and the total integrated intensity of the central transition obeys a simple Curie-Weiss

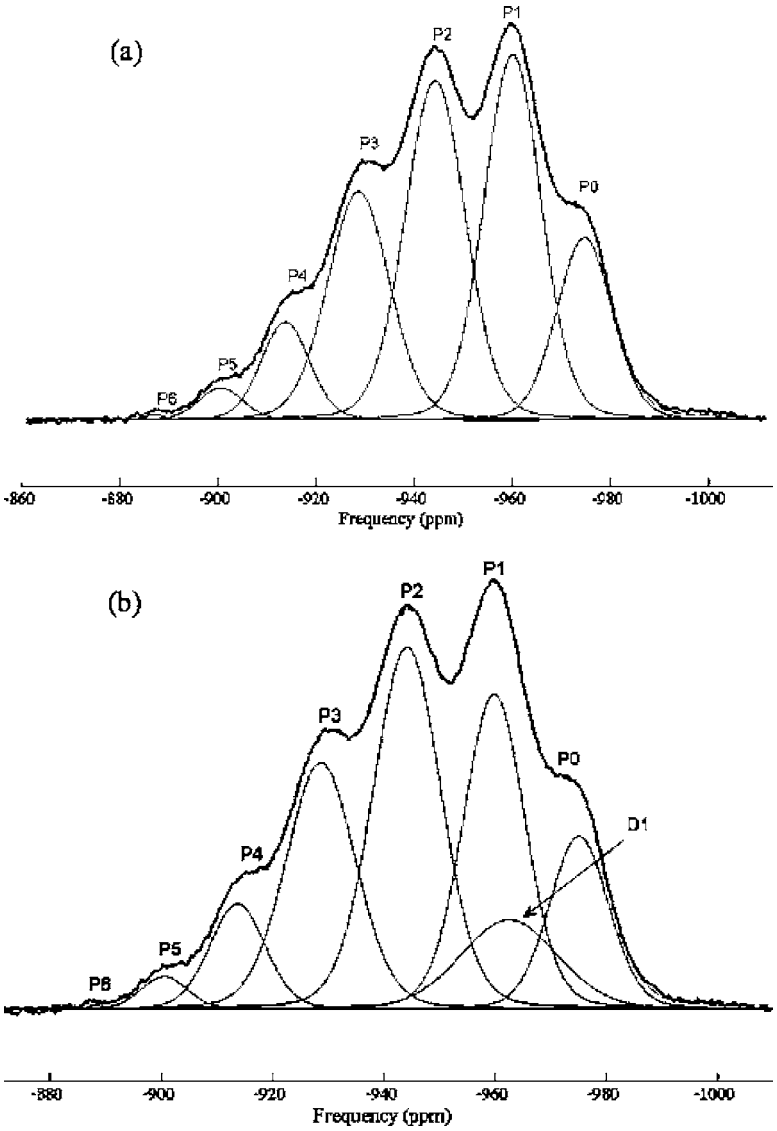

FIG. 3. Deconvolution of the MAS spectrum for 0.4PMN-0.6PSN at 370 K. (a) Unconstrained fit to seven peaks, P0–P6. (b) Constrained fit, including an eighth peak, D1. The position of D1, but not its intensity or width, was determined from 3QMAS experiments as described in the text.

law. This implies that peak D1 must have shifted downfield, so that it is fully masked by the other peaks at 360 K. Similar results are found at other temperatures; D1 is visible as a shoulder in the spectrum only below 290 K, while above that temperature it falls under the sharp peaks. Fortunately, D1 *can* be directly observed at all temperatures in 3QMAS spectra (see below), and its frequency can then be incorporated as a *fixed* parameter for quantitative deconvolution of the MAS spectra. This deconvolution procedure then gives the width and relative intensity of D1, along with the widths, intensities, and center frequencies of peaks P0, P1,…,P6.

The temperature dependence of the best-fit peak positions is shown in Fig. 4.

P5 and P6 are not shown because the total intensity of these peaks for this sample was less than 5% and the values are unreliable. Peaks P0–P4 show a weak, essentially linear temperature dependence, with slope ~ -0.1 ppm/K. However, the temperature dependence of D1 is nonlinear and much stronger: below the temperature of maximum dielectric loss, ~ 310 K,[8] D1 appears as a shoulder on the side of the spectrum, but as temperature increases in the paraelectric phase, D1 shifts up field by about 10 ppm and lies almost underneath P1 at 380 K. This behavior is consistent with our recent results for pure PMN,[21] which implicate the nBn configurations in D1 as major contributors to polar nanoclusters.

B. 0.4PMN-0.6PSN 3QMAS

3QMAS spectra of ^{93}Nb in 0.4PMN-0.6PSN at 260 K (ferroelectric phase) and 365 K (paraelectric phase) are shown in Figs. 5(a) and 5(b), respectively.

Both spectra were processed with shear factor 3. The vertical dashed lines indicate frequencies in F_2 (the direct dimension) that are approximately midway between the MAS peak frequencies of P0 and P1, and corresponding F_1 slices are shown in the insets. These particular slices are displayed to demonstrate that the corresponding regions in the single-quantum MAS spectrum consist of two overlapping components with distinctly different quadrupole coupling parameters. Simulations (not shown) indicate that a Gaussian distribution of quadrupole coupling constants, combined with asymmetry parameters close to 1, yields a nearly Gaussian line shape in F_1 with the peak maximum $\upsilon_1^{\max}$ determined exclusively by the mean-square quadrupole product $\langle P_Q^2 \rangle$:

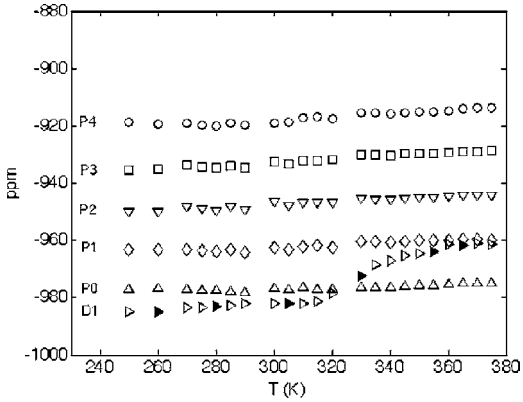

FIG. 4. Temperature dependence of peak positions, determined by deconvolution of ^{93}Nb MAS spectra of 0.4PMN-0.6PSN. The filled symbols represent D1 peak positions extracted with help from 3QMAS experiments as described in the text, and open symbols were determined without recourse to the 3QMAS data.

$$\upsilon_1^{\max} = \frac{3\langle P_Q^2\rangle}{40\upsilon_L^2[2I(2I-1)]^2}[C_Q(3/2,9/2) - 3C_Q(1/2,9/2)]$$

$$= -\frac{27}{20[2I(2I-1)]^2}\frac{\langle P_Q^2\rangle}{\upsilon_L^2}. \quad (2)$$

Thus, decomposing the F_1 slices in Fig. 5 into two overlapping Gaussian peaks yields two P_Q values from each slice: 48±2 MHz and 16.7±1.0 MHz at 260 K and 26.1±1.0 MHz and 13.9±1.0 MHz at 365 K. Each P_Q can be used with Eq. (1b) to compute the contribution of the isotropic second-order quadrupole shift to the corresponding peak frequency in the single-quantum MAS spectrum, and the *observed* single-quantum peak frequencies then yield self-consistent values for the isotropic chemical shifts. Figure 6 shows the temperature dependence of P_Q and δ_{iso}^{cs} determined in this manner for all the resolvable peaks.

Comparing Fig. 6 with Fig. 4, it is evident that the nonlinear temperature dependence of the D1 peak position near T_M arises from both the isotropic chemical shift and the isotropic second-order quadrupole shift.

C. 0.8PMN-0.2PSN VTMAS

The central transition region of a 260 K ^{93}Nb MAS spectrum of 0.8PMN-0.2PSN is shown in Fig. 7.

Previous results[20] show that for the low scandium content of this sample, peaks P0–P3 have negligible intensity. This improves resolution in the region of the distribution peaks, so that D1 and D2 are clearly visible. For this composition, the transition exhibits typical relaxor properties, with a broad transition centered at $T_M \sim 270$ K.[8] Our observations, every 5° between 255 and 365 K, span a significant fraction of the transition region. The temperature dependences of the best-fit peak positions, obtained by deconvolution, are shown in Fig. 8.

Unlike the 0.4PMN-0.6PSN sample, there are no "kinks" in the temperature dependence of any peak position. All are shifted to lower frequency (more negative) with decreasing temperature. For this sample, remnant polarization grows gradually from ~20% at 280 K to 90% at 225 K.[7] The peak positions of D2, P4, P5, and P6 all behave like P0, P1, P2, and P3 in the 0.4PMN-0.6PSN sample, with temperature coefficient of ~−0.1 ppm/K over the measured temperature range. However, the frequency of D1 has stronger temperature dependence than the others, which is consistent with the behavior of this peak in the 0.4PMN-0.6PSN sample. Unfortunately, the sample was lost in a rotor crash before 3QMAS

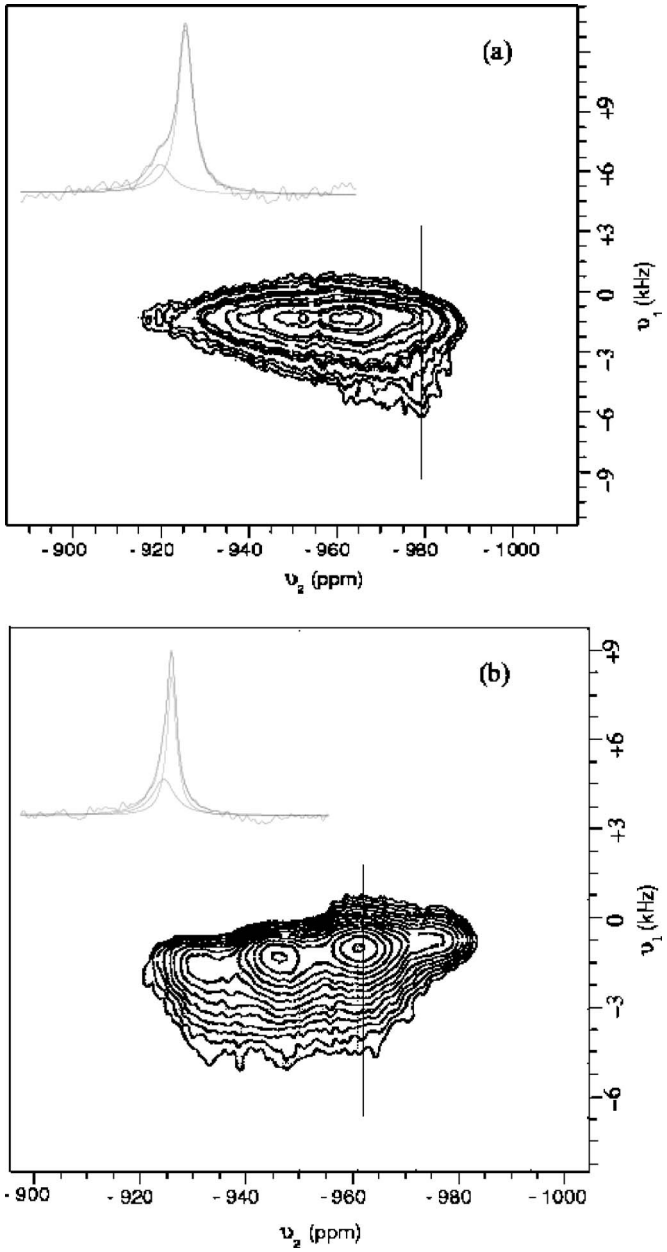

FIG. 5. ^{93}Nb 3QMAS spectra of 0.4PMN-0.6PSN, measured at (a) 365 K and (b) 260 K. The insets show ±9 kHz slices taken along υ_1 at the position indicated by the vertical line. The 3QMAS spectra were processed with shear factor 3, so frequencies along υ_1 are independent of chemical shifts. Deconvolution of the F1 slices thus confirms the existence of peak D1, even when it is not resolved in MAS spectra, and yields an estimate of its isotropic second-order quadrupole shift.

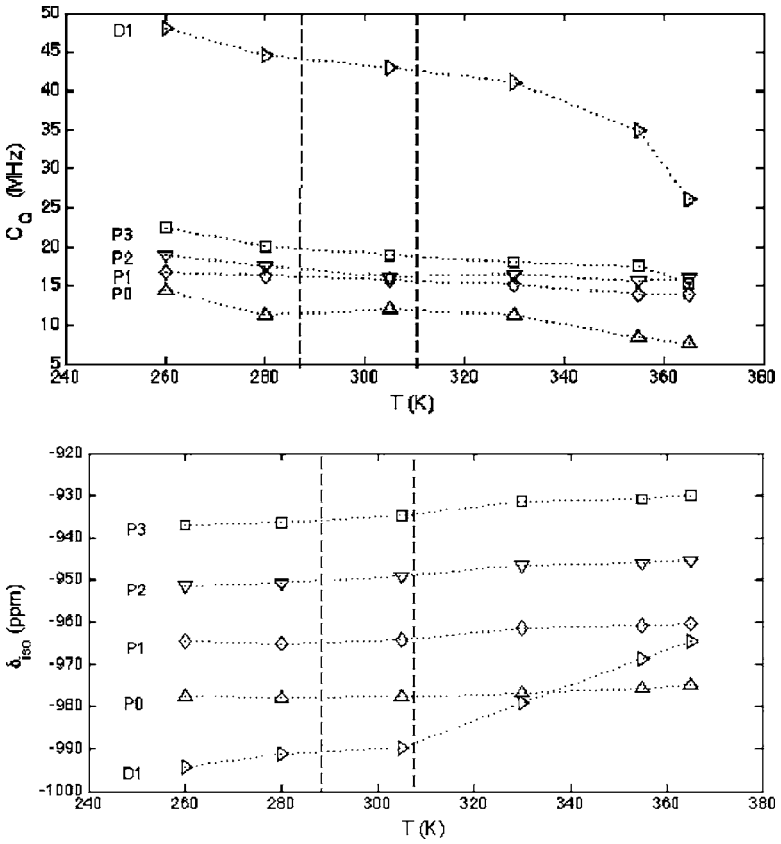

FIG. 6. Temperature dependence of (a) site-specific quadrupole products P_Q and (b) isotropic chemical shifts δ_{iso}^{cs} extracted from variable temperature 3QMAS experiments on 0.4PMN-0.6PSN. Dotted lines connect the symbols to guide the eye. Vertical dashed lines indicate the temperature range (Ref. 7) over which the macroscopic remnant polarization changes between ~10% and 80%.

experiments could be performed to separate the contributions of P_Q and δ_{iso}^{cs}.

IV. DISCUSSION

Extensive measurements[12,15,17,20,28] have established that the chemical shifts and quadrupole coupling parameters of niobium in perovskite and related materials are sensitive to the number and identity of nearest *B*-site neighbors as well as to distortions from exact cubic symmetry. Thus, the temperature dependent site-specific peak frequencies presented in Figs. 4 and 8 report, in general terms, on temperature dependent changes in bond lengths, bond angles, and bond orders of Nb^{5+} cations in specific nBn configurations. The results demonstrate that for both sample compositions, significant geometric distortions in the eleven nBn configurations comprising D1 (see Fig. 2) are associated with the onset of ferroelectricity near T_M. The more gradual changes observed for the 0.8PMN-0.2PSN sample are expected since

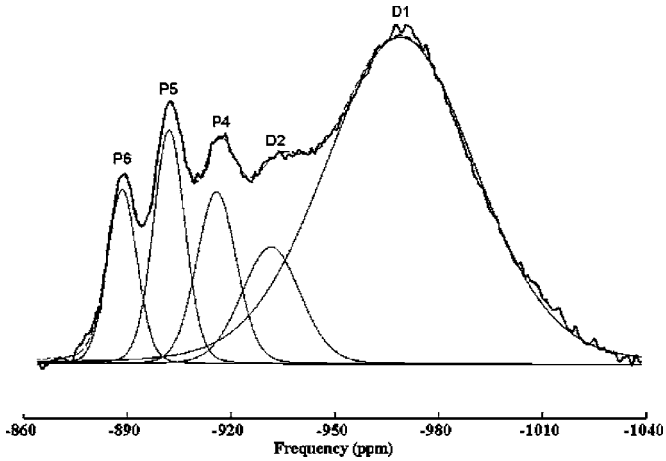

FIG. 7. MAS spectrum of 0.8PMN-0.2PSN at 365 K. The solid line is the experimental spectrum, the thin solid lines identify the best-fit components P0–P6, D1, and D2, and the dashed line (barely visible) is the sum of all the components. Unlike the 0.4PMN-0.6PSN sample, both D2 and D1 are easily determined by deconvolution.

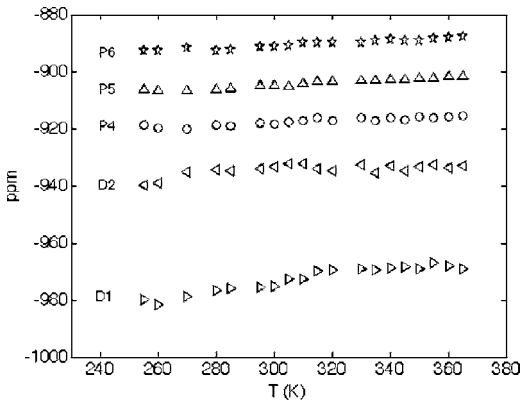

FIG. 8. Temperature dependence of peak positions, determined by deconvolution of ^{93}Nb MAS spectra of 0.8PMN-0.2PSN. The temperature dependence of D1, while larger than that of the other peaks, is weaker than that of the 0.4PMN-0.6PSN sample (see Fig. 4).

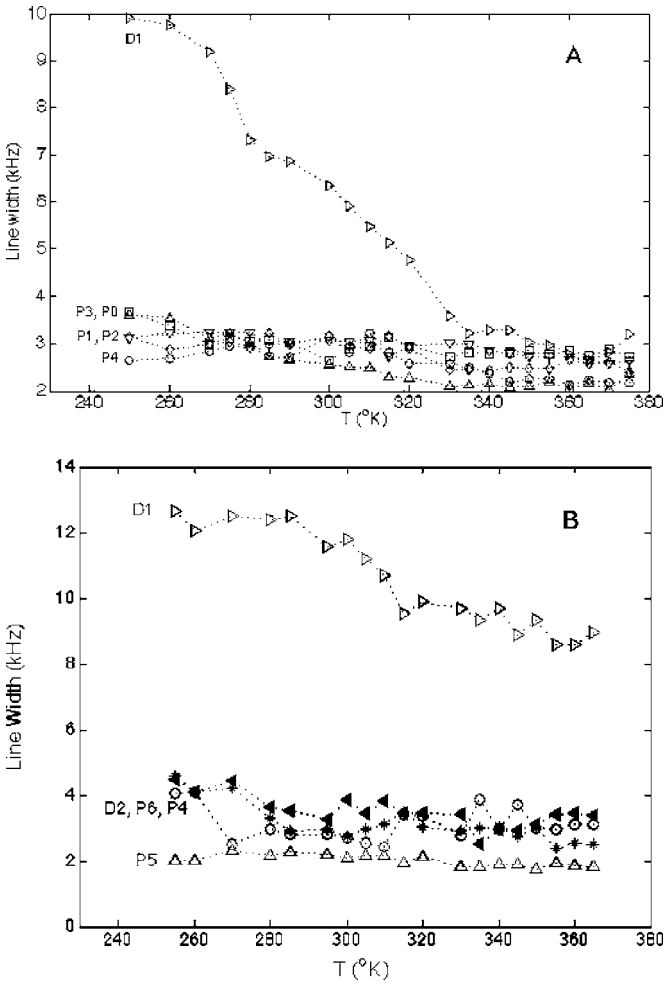

FIG. 9. Site-specific temperature dependent linewidths for (a) 0.4PMN-0.6PSN and (b) 0.8PMN-0.2PSN. In both samples, only D1 is large and temperature dependent.

this low scandium sample is a relaxor. The more abrupt changes, observed for the 0.4PMN-0.6PSN sample, are expected for a normal ferroelectric transition. The vertical bars in Fig. 6 indicate that for the 0.4PMN-0.6PSN sample, remnant polarization drops from ~80% to 20% between ~285 and 305 K.[7] The corresponding range for the 0.8PMN-0.2PSN sample is lower and broader, ~225–280 K.[7]

The local, temperature dependent lattice distortions that influence D1 peak position may reflect the existence of randomly oriented local polarization, in both samples, above the phase transition. Support for this hypothesis is provided by the site-specific, temperature dependent linewidths, shown in Fig. 9.

The linewidths of all peaks *except* D1 fall in the range 2–4 kHz and are almost independent of temperature. For both samples, D1 is much wider, especially below T_M. This is not simply due to the fact that D1 represents an overlap of contributions from different nBn configurations; D2 also represents many different configurations and its linewidth [solid triangles, Fig. 9(b)] remains small at all temperatures.

In pure PMN, the MAS linewidth of D1 *decreases* with decreasing temperature and this was ascribed[21] to more uniform local distortions that accompany increasing polarization of the polar nanoclusters. However, in 0.4PMN-0.6PSN and 0.8PMN-0.2PSN, the MAS linewidth *increases* with decreasing temperature. This difference could be due to the greater diversity of nBn configurations in the PMN-PSN solid solutions, for which D1 includes 11 configurations with at least one Nb^{5+} cation and no more than one Mg^{2+} cation. The MAS linewidths depend on numerous factors, including contributions from distributions of both isotropic chemical shifts and quadrupole coupling parameters, as well as potential contributions from dynamic frequency shifts associated with quadrupole relaxation.[29] There is ample theoretical[30] and experimental[14,31] evidence of the dynamic nature of polar nanoclusters, that can be associated with rapid hops of *B*-site cations (and associated displacements of *A*-site cations) among different off-center positions with respect to the surrounding oxygen octahedra. Unfortunately, we are not able to cool the MAS probe low enough to freeze out such motion for the PMN or PMSN samples, but it is entirely possible that the relatively large linewidths observed for D1 include contributions from this motion. More detailed interpretation is not warranted.

In pure PMN and other relaxor ferroelectrics, it is generally agreed that the local, microscopic electric dipole moments align to produce polar nanoclusters.[32] Blinc and co-workers[13,14] suggest that relevant NMR parameters should therefore depend linearly on the local polarization P_{local}:

$$\delta = \delta_0 + \delta_1 P_{local}. \tag{3}$$

Here, δ is used to denote a generic NMR parameter such as the chemical shift or quadrupole coupling constant of any NMR-active nucleus. δ_0 includes the effects of ferroelectrically *inactive* distortions, while δ_1 represents the net effect of all distortions that produce a local polarization. Equation (3) has been used, for example, to interpret the observed frequencies and linewidths of ^{207}Pb in field-cooled PMN samples in terms of static and dynamic components of the local polarization.[14] According to this interpretation, observed MAS frequencies of D1 would then be given by the sum of two contributions, one involving the isotropic chemical shift δ_{iso}^{CS} and the other the isotropic second-order quadrupole shift δ_{iso}^{2Q}

$$\delta_{\mathrm{D1}}(\mathrm{obs}) = (\delta_{iso,0}^{CS} + \delta_{iso,0}^{2Q}) + (\delta_{iso,1}^{CS} + \delta_{iso,1}^{2Q}) P_{local}. \tag{4}$$

The $(\delta_{iso,0}^{CS} + \delta_{iso,0}^{2Q})$ terms for peak D1 are expected to show the same gentle temperature dependence as the observed peak frequencies, $\delta_{P_i}(\mathrm{obs})$, of those nBn configurations not involved in local ferroelectric domains. Departure form this gentle temperature dependence observed for $\delta_{\mathrm{D1}}(\mathrm{obs})$ is then associated with temperature dependent growth of local polarization.

Before proceeding with this interpretation, it is important to note that Eq. (3) has not, to our knowledge, been experimentally verified. In fact, the data reported in Fig. 6(a) for ^{93}Nb quadrupole coupling constants and in Fig. 6(b) for isotropic chemical shifts provide experimental evidence that Eq. (3) may be an oversimplification. Independent measurements of remnant polarization[8] show that the 0.4PMN-0.6PSN or-

dered sample behaves like a normal ferroelectric material, with a sharp change in remnant polarization near $T=275$ K. However, Fig. 7(a) shows that the isotropic chemical shift does not change significantly until $T=\sim 305$ K and the quadrupole coupling constant begins to decrease sharply only above ~330 K. These differences are not surprising; the remnant polarization is a macroscopic property that represents a nonzero sum of P_{local} averaged over the whole sample. The fact that both C_Q and δ_{iso}^{CS} retain their low-temperature values well above 275 °K simply implies that local, microscopic domains with randomly oriented local polarization remain above this temperature.

Of more concern is the fact that the nonlinear drop in C_Q with increasing temperature occurs ~25° above the point where δ_{iso}^{CS} starts to increase. This behavior is *not* consistent with Eq. (4), which ascribes all observed temperature dependence in both NMR parameters to distortions that also produce local electric dipole polarization. However, it is easy to envision symmetric distortions of the oxygen octahedra surrounding each Nb^{5+} cation that produce an electric-field gradient but no net electric dipole moment. Independent evidence that such distortions are possible is available from studies of crystalline niobium compounds which demonstrate that δ_{iso}^{CS}, but not C_Q, can be used to determine the Nb-O coordination number.[12] Moreover, early measurements of ^{93}Nb pure quadrupole resonance in potassium niobate combined with point-charge calculations of electric-field gradients[33] suggest that the quadrupole coupling constant should vary as the square of the macroscopic polarization. We conclude that at least for ^{93}Nb, the use of Eq. (4) to assess local polarization from the temperature dependence of measured peak frequencies is at best dubious.

The NMR parameters for D1 reveal qualitatively different behavior for 0.8PMN-0.2PSN (a relaxor) and 0.4PMN-0.6PSN (a normal ferroelectric). In particular, the absence of a sharp kink in the temperature dependence of the D1 peak frequency of the 0.8PMN-0.2PSN sample, combined with a gradual increase in integrated intensity of this peak with decreasing temperature, suggests that local distortions characteristic of polar nanoclusters can spread beyond the nBn configurations nominally included in D1.

Although the "measured" relative intensities are subject to large uncertainty due to difficulties in deconvoluting overlapping peaks with different widths, it is interesting to use the random site model to estimate the relative amount of individual nBn configurations that are lumped together in D1. In the 0.4PMN-0.6PSN sample, the random site model predicts that 93.5% of the total intensity of D1 is divided between five of the 11 nBn configurations: (Nb,Sc,Mg)=(6,0,0) with 29%; (1,4,1) with 30%; and (1,5,0),(2,4,0), and (2,3,1) with 13.6%, 7.5%, and 13.4%, respectively. There is *less* diversity for $x=0.2$, where the (6,0,0) configuration accounts for 77% of the Nb^{5+} cations in D1, with 5% in the (3,2,1) configuration and 4.7% in (5,0,1). The Nb^{5+} cation (ionic radius of 0.69 Å) is smaller than Sc^{3+} (ionic radius of 0.745 Å) or Mg^{2+} (ionic radius of 0.72 Å), and this facilitates large, off-center distortions with an accompanying large, easily reorientable polarization in this configuration. In the $x=0.6$ sample, a normal ferroelectric, the random site model prediction for the (6,0,0) intensity is only 11.8%. For $x=0.2$, a relaxor, the random site prediction for the (6,0,0) intensity is 21%. This suggests that the relaxor behavior observed for low scandium content is not due solely to a diversity of local configurations with different transition temperatures, but also to the ability of the highly polar (6,0,0) configuration to induce further distortions in its immediate surroundings. This configuration can be regarded as a nucleus for formation of the polar nanoclusters.

V. CONCLUSIONS

Variable temperature ^{93}Nb MAS and 3QMAS NMR experiments have been performed on perovskite relaxor ferroelectric PMN-PSN solid solutions at high magnetic field (17.6 T). Based on previous assignments of partially resolved peaks to specific configurations of nearest *B*-site neighbor configurations, the observed temperature dependence of the NMR parameters confirms the previous conclusion[21] that nBn configurations with more than one Mg^{2+} cation do not participate in the cooperative distortions that lead to bulk ferroelectricity. Analysis based on the random site model for nBn configurations suggests that in these samples, the crossover between relaxor and normal ferroelectric behavior is determined, at least in part, by the amount of the highly polar, easily deformable nBn configuration with six Nb^{5+} cations.

ACKNOWLEDGMENTS

This work was supported by the Office of Naval Research, Contract No. N000140310661, and the National Science Foundation, Grant No. CHE0079136. We thank Peter Davies (U. Penn) for providing the PMN-PSN samples and for many useful discussions.

*Corresponding author. Electronic address: rlvold@wm.edu

[1] Z.-G. Ye, Key Eng. Mater. **155-6**, 81 (1998).
[2] L. E. Cross, Ferroelectrics **151**, 305 (1994).
[3] I. W. Chen, J. Phys. Chem. Solids **61**, 197 (2000).
[4] L. E. Cross, Ferroelectrics **76**, 241 (1987); D. Viehland, J. F. Li, S. J. Jang, L. E. Cross, and M. Wuttig, Phys. Rev. B **43**, 8316 (1991).
[5] E. V. Colla, E. Y. Koroleva, N. M. Okuneva, and S. B. Vakhrushev, Phys. Rev. Lett. **74**, 1681 (1995).
[6] R. Pirc and R. Blinc, Phys. Rev. B **60**, 13470 (1999).
[7] L. Farber, M. Valant, M. A. Akbas, and P. K. Davies, J. Am. Ceram. Soc. **85**, 2319 (2002).
[8] L. Farber and P. K. Davies, J. Am. Ceram. Soc. **86**, 1861 (2003).
[9] V. Shuvaeva, I. Pirog, Y. Azuma, K. Yagi, K. Sakaue, H. Terauchi, I. P. Raevskii, K. Zhuchkov, and M. Y. Antipin, J. Phys.: Condens. Matter **15**, 2413 (2003).

[10] W. Dmowski, M. K. Akbas, P. K. Davies, and T. Egami, J. Phys. Chem. Solids **61**, 229 (2000).
[11] F. Fayon, I. Farnan, C. Bessada, J. Coutures, D. Massiot, and J. P. Coutures, J. Am. Chem. Soc. **119**, 6837 (1997).
[12] O. B. Lapina, D. F. Khabibulin, K. V. Romanenko, Z. Gan, M. G. Zuev, V. N. Krasil'nikov, and V. E. Fedorov, Solid State Nucl. Magn. Reson. **28**, 204 (2005).
[13] R. Blinc, V. V. Laguta, V. Zalar, and J. Banys, J. Mater. Sci. **41**, 27 (2006).
[14] R. Blinc, Ferroelectrics **330**, 1 (2006).
[15] G. L. Hoatson, D. H. Zhou, F. Fayon, D. Massiot, and R. L. Vold, Phys. Rev. B **66**, 224103 (2002).
[16] J. J. Fitzgerald, J. Huang, and J. S. Shore, Ferroelectrics **233**, 187 (1999).
[17] J. J. Fitzgerald, S. Prasad, J. Huang, and J. S. Shore, J. Am. Chem. Soc. **122**, 2556 (2000).
[18] M. D. Glinchuk, V. V. Laguta, I. P. Bykov, S. Nokhrin, V. P. Botvun, M. A. Leschenko, J. Rosa, and L. Jastrabik, J. Appl. Phys. **81**, 3561 (1997).
[19] V. V. Laguta, M. D. Glinchuk, S. N. Nokhrin, I. P. Bykov, R. Blinc, A. Gregorovic, and B. Zalar, Phys. Rev. B **67**, 104106 (2003).
[20] D. H. Zhou, G. L. Hoatson, and R. L. Vold, J. Magn. Reson. **167**, 242 (2004).
[21] M. Vijayakumar, G. L. Hoatson, and R. L. Vold, Phys. Rev. B **75**, 104104 (2007).
[22] P. K. Davies, L. Farber, M. Valant, and M. A. Akbas, AIP Conf. Proc. **535**, 38 (2000).
[23] J.-P. Amoureux, C. Fernandez, and S. Steuernagel, J. Magn. Reson., Ser. A **123**, 116 (1996).
[24] T. Charpentier, C. Fermon, and J. Virlet, J. Chem. Phys. **109**, 3116 (1998).
[25] L. Frydman and J. S. Harwood, J. Am. Chem. Soc. **117**, 5367 (1995).
[26] D. Massiot, F. Fayon, M. Capron, I. King, S. Le Calve, B. Alonso, J.-O. Durand, B. Bujoi, Z. Gan, and G. L. Hoatson, Magn. Reson. Chem. **40**, 70 (2002).
[27] M. K. Akbas and P. K. Davies, J. Am. Ceram. Soc. **83**, 159 (2000).
[28] S. Prasad, P. Zhao, J. Huang, J. J. Fitzgerald, and J. S. Shore, Solid State Nucl. Magn. Reson. **19**, 45 (2001); H. Fitzgerald and J. Shore, presented at the 41st ACS Symposium on Solid State NMR, Denver, CO 1999 (unpublished).
[29] A. Abragam, *Principles of Nuclear Magnetism* (Clarendon, Oxford, 1961); A. Baram, Z. Luz, and S. Alexander, J. Chem. Phys. **58**, 4558 (1973).
[30] B. E. Vugmeister, Phys. Rev. B **73**, 174117 (2006).
[31] B. E. Vugmeister and H. Rabitz, Phys. Rev. B **57**, 7581 (1998).
[32] G. Burns and F. H. Dacol, Solid State Commun. **48**, 853 (1983); J. Toulouse, D. La-Orauttapong, and O. Sviitelskiy, Ferroelectrics **302**, 271 (2004); I.-K. Jeong, T. W. Darling, J. K. Lee, T. Proffen, R. H. Heffner, J. S. Park, K. S. Hong, W. Dmowski, and T. Egami, Phys. Rev. Lett. **94**, 147602 (2005).
[33] R. R. Hewitt, Phys. Rev. **121**, 45 (1961).